

INVESTIGATION OF FINE STRUCTURE OF POTASSIUM EMISSION SPECTRUM
IN RUBY LASER FIELD

V. A. GOLUBEV, Yu. M. KIRIN, D. P. KOVALEV, S. G. RAUTIAN, and B. M. CHERNOBROD

Institute of Semiconductor Physics, Siberian Department, USSR Academy of Sciences

Submitted March 5, 1970

Zh. Eksp. Teor. Fiz. 59, 661-672 (September, 1970)

The fine structure of potassium atom emission spectrum at $\lambda = 4044/47 \text{ \AA}$ ($5P_{3/2,1/2} - 4S_{1/2}$ transition) is investigated in an intense ruby laser field and Stokes SRS radiation of nitrobenzene. The observed structure is found to depend strongly on the field intensity and vapor pressure. As a result the conclusion is made that field splitting of energy levels is the basic factor determining the structure of the $\lambda = 4044/47 \text{ \AA}$ lines. Its theoretical interpretation is given by the "three-strong-fields model." The number of the fine structure components and the line shift relative to the atomic transition frequency obtained in the experiment are compared with theoretical values. Multiphoton emission lines shifted relative to the $5P - 4S$ transition frequency towards lower and higher frequencies are observed and explained.

1. INTRODUCTION

RECENTLY, a large number of reports were published on the propagation of high power radiation through a resonance medium. The resonance nature of the interaction between strong fields and atoms leads to a variety of effects such as shifting and splitting of atomic levels, broadening of the emission spectrum that passed through a medium, and a high probability of multiphoton processes of absorption, emission, and scattering of light. These were reviewed in detail in^[1-3]. The rarity of media with energy level transition frequency close to that of high power laser emission is the reason for the large amount of research performed with potassium vapor. The frequency ω_{21} of the $6S_{1/2} - 4P_{3/2}$ transition of a potassium atom (Fig. 1) is close to frequency ω_R of ruby laser emission ($\omega_{21} = 14407.1 \text{ cm}^{-1}$, $\omega_R = 14399.3 \text{ cm}^{-1}$) while frequency ω_{10} of the $4S_{1/2} - 4P_{3/2}$ resonance transition is close to Stokes SRS frequency ω_S of this emission in nitrobenzene ($\omega_{10} = 13042.9 \text{ cm}^{-9}$, $\omega_S = 13055 \text{ cm}^{-1}$).

Simultaneous irradiation of potassium atoms by the ruby laser emission and its Stokes SRS component in nitrobenzene significantly populates levels $4P_{3/2,1/2}$ (1, 1'), $6S_{1/2}$ (2), $5P_{3/2,1/2}$ (3, 3') and $4D_{5/2,3/2}$ (4) (Fig. 1) due to the single- or two-quantum absorption of photons with frequencies ω_R and ω_S and their Raman scattering. All observers working under these conditions report an intense directed emission at frequencies ω_{23} , ω'_{23} , and $\omega_2 = \omega_R - \omega_{31}$, $\omega_4 = \omega_R - \omega'_{31}$, in the infra-red spectral region, as well as at ω_{30} , ω'_{30} , ω_{10} , and ω'_{10} in the visible region^[4-13]. According to^[10,11] violet lines ω_{30} and ω'_{30} had an anomalously broad spectrum with a "dip" in the center of the line, while red lines ω_{10} and ω'_{10} were shifted $1.5-2 \text{ cm}^{-1}$ towards longer waves relative to the atomic transition.

In the present paper we describe the results of investigating potassium vapor emission spectrum in the region of violet lines ω_{30} and ω'_{30} ($\lambda = 4044/47 \text{ \AA}$). Emission in this region consists of three groups of lines:

1. Comparatively weak lines shifted a few tens of

cm^{-1} towards longer waves relative to ω_{30} (they are henceforth called "long-wave lines");

2. Emission whose wavelength is shorter than ω_{30} and whose spectral structure varies with conditions ("short-wave lines");

3. Lines ω_{30} and ω'_{30} with complex structure.

We were mainly interested in the fine structure of lines $\lambda = 4044/4047 \text{ \AA}$, which depends strongly on the potassium vapor pressure and the power of the laser and SRS emissions. The observed structure is interpreted as a consequence of one of the basic effects of non-linear spectroscopy, i.e., splitting of atomic levels in electromagnetic field^[2]. The essential difference between our case and the recognized manifestations of this effect^[1,14,15] consists in the fact that potassium atoms are exposed to a field whose spectrum contains several monochromatic lines splitting the level into many components (rather than into two as in a monochromatic field).

2. THE EXPERIMENTAL SETUP

Figure 2 shows a diagram of the experimental setup. Laser emission from ruby 1 with passive shutter 2

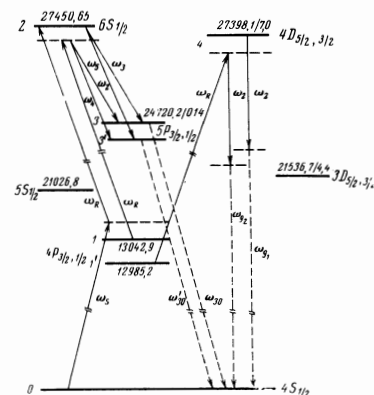


FIG. 1. Diagram of potassium terms. Solid arrows correspond to "strong fields," dashed arrows designate potassium emission lines in the violet spectral range.

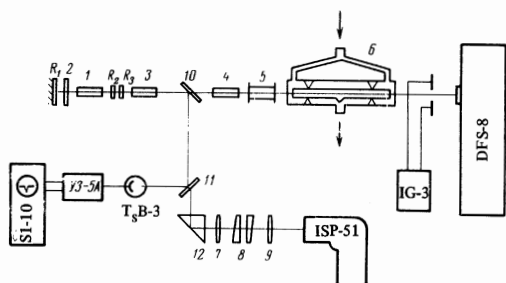


FIG. 2. Diagram of experimental setup. 1—ruby laser; 2—phototropic shutter; 3, 4—ruby laser amplifier; 5—nitrobenzene cell; 6—potassium cell; 7, 9—lenses; 8—Fabry-Perot etalon (IT-51-30); 10, 11—plane-parallel beam splitters; 12—prism; R_1 —mirror; R_2 , R_3 —glass and sapphire plane-parallel plates respectively.

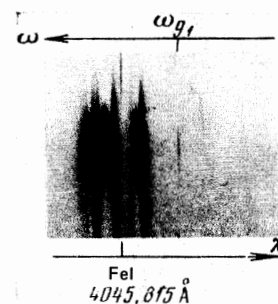
(K-19 glass or phthalocyanine dye in nitrobenzene with initial transmission of 13%) and power output $P_R = 30$ MW is amplified up to $P_R = 100$ MW by a laser amplifier using rubies 3 and 4. Mirror R_1 ($T = 0.1\%$) and a stack of glass (R_2) and sapphire (R_3) plane parallel plates spaced 0.3 cm from one another formed a resonator with axial mode selection. This in conjunction with the selection properties of phototropic shutters narrowed the laser generation spectrum down to 0.01 cm^{-1} . To monitor the spectral composition of laser emission a portion of the beam was diverted by beam splitter 10 to a Fabry-Perot etalon (IT-51-30) crossed with an ISP-51 (UF-84 camera). The absolute value of laser emission frequency was shifted by varying the temperature of the ruby crystal^[16] ($\omega_R = 14401.6$ cm^{-1} at $t_R = 0^\circ\text{C}$; $\Delta\omega_R/\Delta t \approx -0.135$ $\text{cm}^{-1}/^\circ\text{C}$). Crystal temperature was monitored by a graduated chromel-copel thermocouple connected to an M-95 type galvanometer. The “hot” junctions of the thermocouple were in contact with the lateral surface of the crystal and the “cold” junctions were placed in a vessel with melting ice.

A portion of laser emission was diverted by beam splitter 11 to a TsV-3 photocell. The photocell signal passed through a U3-5A amplifier to the plates of an S1-10 oscilloscope. This allowed us to determine the length of the laser generation pulse which turned out to be 30 nsec (at one-half amplitude).

The unfocused beam of laser light passed through cell 5 with nitrobenzene and excited there the Stokes component of SRS. The power of this component was determined by the laser emission intensity and amounted to $P_S = 5$ MW for $P_R = 100$ MW. The scattered emission spectrum was broad (several cm^{-1}). Furthermore, stimulated Mandel'stam-Brillouin scattering (SMBS) also was excited in the nitrobenzene cell. We observed Stokes and anti-Stokes components of SMBS and their harmonics, shifted 0.2 cm^{-1} from ω_R . At high laser powers the intensity and width of SMBS components were comparable to those of the laser emission line.

The laser, SRS, and SMBS emissions propagated simultaneously along the axis of cell 6 containing saturated potassium vapor. The cell was a tube of molybdenum glass 16 mm in diameter and 600 mm long fitted with sapphire windows and placed within a metal jacket with end-face windows. The reason for the sapphire windows was the fact that sapphire does not interact with potassium and thus ensures a protracted availabil-

FIG. 3. Spectrogram of multiphoton emission lines shifted in the long-wave direction relative to the frequency of the 5P-4S transition (“long-wave lines”).



ity of clean windows. Glass, however, darkens rapidly at 200 – 300°C (owing to chemical interaction of potassium atoms with glass components). The glass tube was first evacuated to 10^{-5} Torr and then filled with distilled (to remove impurities) metallic potassium. Next the tube was cut off from the vacuum nozzle and inserted in the metal tube, leaving a 3–5 mm air gap between the glass (with potassium) and metal tubes for the passage of heated air to bring the potassium up to 100 – 350°C . To prevent potassium from condensing on the windows the jet of hot air from the heater was first directed against the windows and then allowed to pass the remainder of the tube (Fig. 2). In this arrangement the air temperature was 30 – 40°C higher at the windows than in the other parts of the tube. The potassium cell temperature was measured with a graduated chromel-copel thermocouple connected to an M-194 galvanometer. The “hot” junctions of the thermocouple were placed at the air exit from the cell, and the “cold” junctions were immersed in a vessel with melting ice.

The emission spectrum from the potassium vapor cell was photographed with a DFS-8 spectrograph (second-order dispersion 1.37 $\text{\AA}/\text{mm}$ (or 8.5 cm^{-1}/mm in the violet region), instrument width 0.15 cm^{-1}) on RF-3 film or “Infra-760” plate. The absolute values of fine structure frequencies of the recorded lines were determined from base lines of iron spectrum obtained with an IG-3 spark generator. An Abbe comparator was used to measure the line positions. The accuracy of measurements depended on the comparatively large line widths and amounted to 0.5 cm^{-1} .

3. EXPERIMENTAL RESULTS

A. Long-wave Lines

The spectrogram in Fig. 3 shows a line whose frequency is designated by ω_{g_1} ; two other lines ω_{g_2} and ω_{g_3} that are considered below are not visible in Fig. 3 because of weak intensity. These lines were observed only at $P_R = 100$ MW and $P_S = 5$ MW and pressures of potassium vapor $p = 0.3$ – 0.4 Torr. Their intensity is relatively low and their excitation is not quite stable. Most often we observed one (ω_{g_1}) or two (ω_{g_1} and ω_{g_2}) lines.

The origin of lines ω_{g_1} , ω_{g_2} , and ω_{g_3} is not quite clear. There are two possible hypotheses: stimulated two-quantum luminescence at the $4D_{5/2,3/2} - 4S_{1/2}$ transition, or three-photon scattering in which $4P_{1/2}$ is the initial state and laser (ω_R) and infrared (ω_{23} , ω'_{23} , ω_2) photons participate.

The frequency of transition $4D_{3/2} - 4P_{1/2}$ (14412 cm^{-1})

Frequencies of "long-wave" lines

ω	Measured, cm^{-1}	Computed from (3.1), cm^{-1}	Computed from (3.2), cm^{-1}
ω_{g_1}	24676.4	24675.6	—
ω_{g_2}	24663.0	24667.1	24662.5
ω_{g_3}	24649.0	24648.4	—

differs from $\omega_R = 14399.0 \text{ cm}^{-1}$ only by 13 cm^{-1} and we can assume that the 4D state can be effectively populated. Infrared emission at the 6S – 5P transition (i.e., $\omega_3, \omega_5, \omega_2$) can stimulate a two-quantum transition 4D – 4S giving rise to violet lines. According to this hypothesis we have

$$\omega_{g_1} = \omega_{10} - \omega_2, \quad \omega_{g_2} = \omega_{10} - \omega_3, \quad \omega_{g_3} = \omega_{10} - \omega_5. \quad (3.1)$$

Comparing the measured values of ω_{g_1} with those computed¹⁾ from (3.1) (see the table) we find that there is a good agreement for ω_{g_1} and ω_{g_3} . On the other hand, in the case of the ω_{g_2} line the difference between the measured and computed values ($\sim 4.1 \text{ cm}^{-1}$) is much greater than the possible measurement error.

According to the second hypothesis the ω_{g_1} lines can occur in the course of a three-photon scattering process where a laser emission photon ($\hbar\omega_R$) vanishes and ω_2 and ω_{g_2} photons are emitted, while $4P_{1/2}$ and $4S_{1/2}$ are the initial and final atomic states respectively:

$$\omega_{g_1} = \omega'_{10} + \omega_R - \omega_2. \quad (3.2)$$

The value of ω_{g_2} computed from (3.2) coincides with the measured value within the limits of experimental error. Thus lines ω_{g_1} , ω_{g_2} , and ω_{g_3} seem to occur as a result of processes that are different from the viewpoint of the perturbation theory classification: two-quantum luminescence (ω_{g_1} and ω_{g_3}) and three-photon Raman scattering (ω_{g_2}). On the other hand if we are based on the concept of level splitting^[2,15] in the field of a ruby laser, then lines ω_{g_1} and ω_{g_2} are a consequence of a single process. In fact, one can hold that a field with a frequency ω_R interacts with the $4P_{1/2} - 4D_{3/2}$ transition and "splits" it into two quasi-energy sublevels. One sublevel is located at a distance equal to the detuning $\omega'_{41} - \omega_R$, while the other is near the $4D_{3/2}$ level. The two-quantum emission from these sublevels stimulated by infrared emission with a frequency ω_2 then produces the lines ω_{g_1} and ω_{g_2} .

It may seem strange that what does occur is the fairly complex process described above, while a simpler process such as the one-quantum 4D – 4P transition is not observed. There are two reasons for this. First, according to computation by the Bates-Damgaard^[17] method, the oscillator strength for the 4D – 5P transition is almost three orders higher than that for the 4D – 4P transition (0.64 and 0.0014 respectively). Second, the system is exposed to a powerful infrared radiation close to the 4D – 5P transition frequency (mismatch of $25 - 50 \text{ cm}^{-1}$). Therefore the infraction of "hierarchy" of the processes is perfectly natural.

¹⁾ Computations show that levels $4D_{5/2}$ and $4D_{3/2}$ make a roughly equal contribution to the emission. Therefore the computation from (3.1) was made for a mean energy of the 4D term, i.e., for the frequency of 27397.5 cm^{-1} .

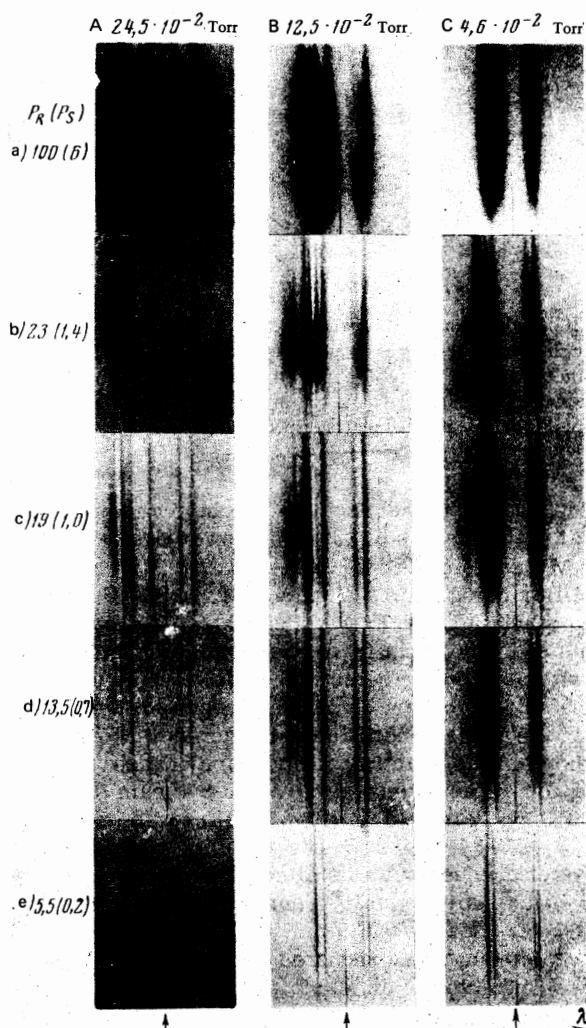


FIG. 4. Variation in structure of lines $\lambda = 4044/47 \text{ \AA}$ (transition $5P_{3/2,1/2} - 4S_{1/2}$) and "short-wave" lines with varying vapor pressures and emission power (MW) of ruby laser and nitrobenzene SRS. Line Fe I 4045.815 \AA is shown by vertical arrows on scale λ ; line ω_{30} \leftrightarrow is to the right, lines ω_{30} , ω_{g_4} and ω_{g_5} to the left.

B. Short-wave Lines

Figures 4–6 show spectrograms in the region of lines ω_{30} and ω'_{30} obtained under various conditions. We now consider radiation situated to the left of line ω_{30} (violet shift). In most spectra we see two lines, one of which is sharp (ω_{g_4}) and the other much broader (ω_{g_5}) (see Fig. 4, B and C, for example). For $\omega_R = 14399.3 \text{ cm}^{-1}$ ($t_R = 16^\circ \text{C}$) the shifts of ω_{g_5} and ω_{g_4} relative to line ω_{30} are 12 and 7.5 cm^{-1} respectively. Under certain conditions (in particular at potassium vapor pressures $p > 0.125 \text{ Torr}$) a "dip" that we consider an absorption line appears near emission line ω_{g_4} . The width of the absorption line increases with rising vapor pressure. As the power of laser and SRS emissions increases line ω_{g_5} broadens and, when $P_R = 50 \text{ MW}$ and $P_S = 2 \text{ MW}$ and above, its low-frequency wing overlaps the high-frequency wing of line ω_{30} (Fig. 4, Aa). The width of the absorption line increases at the same time.

Line ω_{g_5} should be interpreted as the result of four-

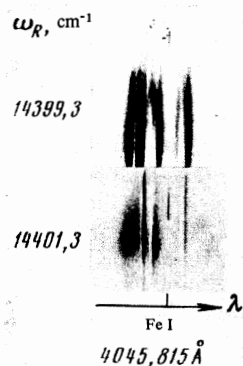


FIG. 5. Change in the location of "short-wave lines" with changing laser emission frequency.

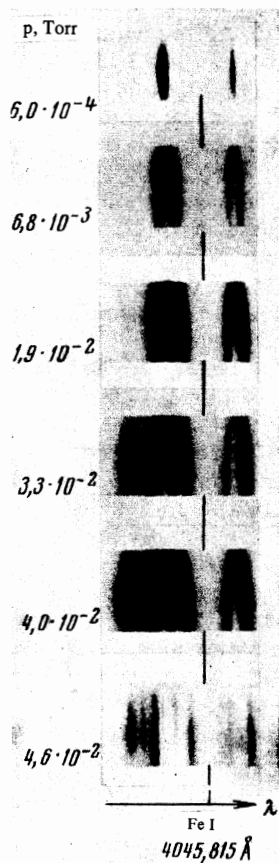


FIG. 6. Variation in the structure $\lambda = 4044/47 \text{ \AA}$ in the "short-wave lines" with varying potassium vapor pressure.

photon processes in which the laser emission photons ω_R and the nitrobenzene SRS photons ω_S vanish, while an infrared photon ω_2 and a violet photon ω_{g_5} are emitted:

$$\omega_{g_5} = \omega_R + \omega_S - \omega_2. \quad (3.3)$$

The width of this line is due to the large width of the SRS spectrum (several cm^{-1}) and its maximum (24732 cm^{-1}), fully conforming to (3.3), corresponds to frequency ω_S of the SRS line maximum.

The sharp line ω_{g_4} can be regarded as a special case of the same process (3.3) in which the sum of frequencies of SRS and the laser field coincides with the $6S_{1/2} - 4S_{1/2}$ transition frequency ($2 - 0$):

$$\omega_{g_4} = \omega_{20} - \omega_2. \quad (3.4)$$

The relative sharpness of line ω_{g_4} is due in this view-

point to the resonance of two-quantum absorption of photons ω_R and ω_S . The value $\omega_{g_4} = 24728.7 \text{ cm}^{-1}$ computed from (3.4) coincides with the measured value (24727.7 cm^{-1}) with an accuracy of 1 cm^{-1} .

It appears from (3.3) and (3.4) that when ω_R increases by $\delta\omega_R$, the frequency ω_{g_5} should increase and ω_{g_4} decrease by $\delta\omega_R$ (the frequencies ω_S and ω_2 contain ω_R as a term). Experiment (thermal scanning of ω_R) confirms this conclusion both in terms of the sign (see Fig. 5) and in terms of the value of shifts within the limits of measurement error $\delta\omega_{g_5} = -\delta\omega_{g_4} = \delta\omega_R$.

A satellite line analogous to ω_{g_4} was observed also on the short-wave side of line $\lambda = 4047 \text{ \AA}$. Its frequency $\omega_{g_6} = 24708.9 \text{ cm}^{-1}$ differs from the transition frequency by 7.5 cm^{-1} and the shift varies following the laser frequency analogously to ω_{g_4} . The relative weakness of line ω_{g_6} (it is observed only when $P_R = 50-70 \text{ MW}$, $P_S = 1-2 \text{ MW}$, and pressure $p = 2.4 \times 10^{-2} \text{ Torr}$) indicates a lower intensity of infrared radiation at the frequency (ω_4).

C. Structure of Line $4044/47 \text{ \AA}$ ($5P_{3/2,1/2} - 4S_{1/2}$)

Figure 4 shows that the structure of line ω_{30} is fairly complex and strongly dependent on the laser field power and vapor pressure. At low pressures and weak powers the center of markedly asymmetric lines has a single sharp dip (Fig. 4 Ce). As powers P_R and P_S increase the dip first widens and then splits successively into two, three, and more components. When $P_R = 100 \text{ MW}$ the line structure becomes quite unsharp and inhomogeneous along the line height. Line ω'_{30} has an asymmetry in the other direction (as compared to ω_{30}) and its dip split is less pronounced; the dip is as a rule single and rarely double.

Variation of vapor pressure with fixed laser power yields a qualitatively similar picture. Figure 6 shows spectrograms obtained for $P_R = 60 \text{ MW}$ within the pressure interval of $p = 0.6 \times 10^{-3} - 0.046 \text{ Torr}$. As pressure increased the dip in line ω_{30} changed successively into a double and triple dip. When $p > 0.2 \text{ Torr}$ the absorption increased to the point (Fig. 4 A) where the structure was invisible and the absorption line very broad. An exception is the case of large P_R and P_S when the structure is retained.

We attribute these changes in line ω_{30} to field splitting of level $5P_{3/2}$ into "quasi-energy sublevels." Apparently both the laser (ω_R) and the infrared (ω_2, ω_3) emissions play a significant role in this effect. This viewpoint explains the effects of pressure: the increasing number of atoms increases the coefficient of conversion of the SRS and laser fields into infrared emission increasing its power, while variation of vapor pressure and power P_R results in analogous effects. The variation in line structure along the slit can be attributed to the transverse inhomogeneity of the initial ruby laser beam and the SRS. The number of spectral components resulting from splitting of the absorption line is also in good agreement with the hypothesis of the field origin of the structure. We consider this point in greater detail.

The above investigation of "long-wave" and "short-wave" lines shows that the laser field (ω_R) and infrared lines (ω_2, ω_3) are the most intense components of the

emission spectrum interacting with potassium atoms. If only these three fields are taken into account, then according to perturbation theory the following three processes are possible that can lead to the absorption of emission in the vicinity of the frequency $\omega = \omega_{20}$: one-quantum absorption of photon $\hbar\omega$, $4S_{1/2} - 5P_{3/2}$; two-quantum absorption of photons $\hbar\omega$ and $\hbar\omega_3$, $4S_{1/2} - 5P_{3/2} - 6S_{1/2}$; and three-quantum process (of the Raman scattering type) with absorption of photons $\hbar\omega$ and $\hbar\omega_2$ and emission of a laser-frequency photon $\hbar\omega_R$, $4S_{1/2} - 5P_{3/2} - 6S_{1/2} - 4P_{3/2}$. Thus the absorption line for the $4S_{1/2} - 5P_{3/2}$ transition is triply degenerate in terms of the "three-strong-fields model" ($\omega_R, \omega_3, \omega_2$). If the intensities are high enough the above processes can no longer be considered independent, the degeneracy is removed, and the line is split into three components.

The calculation based on these considerations is presented in the Appendix. We find that the frequencies of the maxima of absorption line components are given by the following formulas with an accuracy to terms containing squared field amplitudes:

$$\omega^{(1)} \approx \omega_{30} + \Omega_R - \Omega_2 + G_R^2 / \Omega_R, \quad (3.5)$$

$$\Omega_R = \omega_R - \omega_{21}, \quad \Omega_2 = \omega_2 - \omega_{23};$$

$$\omega^{(2,3)} \approx \omega_{30} - \Omega_3 / 2 \pm G_3 - G_R^2 / 2\Omega_R,$$

$$\Omega_3 = \omega_3 - \omega_{23}, \quad G_3 = |d_{23}E_3| / 2\hbar, \quad G_R = |d_{21}E_R| / 2\hbar. \quad (3.6)$$

Here ω_{mn} and d_{mn} are the frequency and matrix element of the dipole moment of the particular transition that interacts with fields ω_j and ω_R with amplitudes E_j and E_R (Fig. 1). The frequency of the photon generated in Raman scattering has a field shift, i.e., $\Omega_2 = \Omega_R + G_R^2 / \Omega_R$ ^[15]. We also can expect a field shift of line ω_3 so that $\Omega_3 = -G_R^2 / \Omega_R$. Therefore we have

$$\omega^{(1)} \approx \omega_{30}, \quad \omega^{(2,3)} \approx \omega_{30} \pm G_3. \quad (3.7)$$

If the fields are weak enough the line components are not resolved and a single absorption line is observed experimentally. However if the ω_3 field is sufficiently intense three components should be visible as in the majority of spectrograms in Fig. 4. Measuring the locations of absorption line components yielded the following results (the base line was Fe I, $\omega = 24709.94 \text{ cm}^{-1}$ shown at the bottom of all spectra). The central component coincides with the location of ω_{30} with an accuracy to $0.1\text{--}0.3 \text{ cm}^{-1}$. Side components are mostly symmetric as required by (3.7) for ω ^[2,3]; there are also, however, deviations from symmetry, reaching $1.5\text{--}2 \text{ cm}^{-1}$. A particularly clear asymmetry occurs at the point of generation of the shorter-wave component (see for example the spectrogram in Fig. 4 Bd). This discrepancy can be ascribed to several causes. Most probably the asymmetry is due to a field shift caused by the Stokes SRS of nitrobenzene and not accounted for in the analysis. It is also possible that the four-photon scattering had some effect (see below).

According to (8) in the Appendix the absorption spectrum represents a set of equidistant triplets (index m) separated by $|\Omega_2 - \Omega_3|$, or 8.5 cm^{-1} ($t_R = 16^\circ\text{C}$) in our experiment. Triplet $m = 0$ determines the structure of line 4044 \AA , while triplet $m = -1$ is associated with the "short-wave line" region. Consequently the structure of the absorption coefficient in the short-wave region should simulate the structure of the $\lambda = 4044 \text{ \AA}$ line itself. Such a congruence is actually observed at suffi-

ciently high pressures and powers P_R and P_S , as can be seen from the spectrograms in Fig. 6 for the pressures of 3.3×10^{-2} , 4.0×10^{-2} , and 4.6×10^{-2} Torr. Measurements showed that the distances between components within each triplet are approximately equal (with an accuracy to $1\text{--}1.5 \text{ cm}^{-1}$). The fact that the structure on the short-wave side appears at higher p , P_R , and P_S is quite understandable since it is the effect of (using perturbation theory language) higher-order processes such as two-, three-, and five-photon processes.

Under certain conditions the number of observed components of the $\lambda = 4044 \text{ \AA}$ absorption line becomes more than three. This is easy to explain if we consider not only the laser emission ω_R and emissions resonating with the $6S_{1/2} - 5P_{3/2}$ transition (ω_2 and ω_3), but also their analogs for the $6S_{1/2} - 5P_{1/2}$ transition (ω_4 and ω_5) and the emission due to transitions from level $5P_{3/2,1/2}$ to lower levels $5S_{1/2}$ and $3D_{5/2,3/2}$. For example we can readily show that given five monochromatic fields $\omega_R, \omega_2, \omega_3, \omega_4$, and ω_5 , the $4S_{1/2} - 5P_{3/2}$ absorption line can split off into eight components.

So far we have not considered the mechanism of generating violet lines. The answer is close at hand and very simple. First, two-quantum absorption of laser emission and SRS (ω_R, ω_S) leads to the population of level $6S_{1/2}$, a population inversion occurs at transitions $6S_{1/2} - 5P_{3/2,1/2}$, and an emission at frequencies ω_3 and ω_5 is generated and amplified. This results in the population of term 5P and generation of lines $\lambda = 4044/47 \text{ \AA}$ at the transition $5P_{3/2,1/2} - 4S_{1/2}$ (Fig. 1). Another mechanism of populating levels $5P_{3/2,1/2}$ is represented by Raman scattering (ω_2, ω_4) of laser emission ω_R in which $4P_{3/2}$ is the initial and $5_{3/2,1/2}$ the final atomic state.

While the above processes are undoubtedly important, they are obviously not unique. The problem is that violet emission (ω_{30} and ω'_{30}) is sharply directed; furthermore it is oriented exclusively in the same direction as nitrobenzene SRS and ruby laser emission. This fact has no obvious explanation from the viewpoint of the above "cascade" hypothesis. We think that the singular direction of this emission is due to the possible role of four-photon scattering ("light-by-light scattering")

$$\omega_S + \omega_R \rightarrow \omega_2 + \omega, \quad (3.8)$$

that is particularly effective when the wave vector condition

$$\mathbf{k}_S + \mathbf{k}_R = \mathbf{k}_3 + \mathbf{k} \quad (3.9)$$

is satisfied (see^[18] for example). Relation (3.9) naturally explains the singular direction of emission at ω_{30} and ω'_{30} ; therefore process (3.8), (3.9) should be significant if at least in the initial generation stages of infrared and violet emissions.²⁾ On the other hand, the cascade mechanism apparently amplifies the light "born of" the four-photon scattering (3.8), (3.9).

It was noted above that the "short-wave lines" ω_{g_4} and ω_{g_5} are also due to the four-photon process. The difference between (3.3) and (3.8), (3.9) consists of the

²⁾By virtue of resonance conditions the four-photon processes of the (3.8), (3.9) type can be quite effective regardless of the low density of atoms ($\sim 10^{15} - 10^{16} \text{ cm}^{-3}$). We showed this in^[19] using the example of potassium vapor transmitting nitrobenzene SRS excited by ruby laser.

fact that (3.3) begins to appear only after the formation of a strong ω_2 field. On the other hand, process (3.8), (3.9) serves as a spontaneous "primer" that gives rise to the field ω_3 and to violet lines.

Simple computation shows that in our doubly resonant conditions we must take into account the fact that the refraction index n differs from unity. It can be readily found that $n - 1 < 0$ for all four frequencies present in (3.8) (except perhaps for ω_R). Therefore to determine the "length of coherent interaction" it is not enough to invoke general considerations but it is necessary to know population differences in all four transitions. The interaction length is quite probably also limited by other factors: absorption, length of coherent train in nitrobenzene SRS emission (~ 0.5 mm) and the difference in group velocities, etc. Because of this the results of theoretical analysis of process (3.8), (3.9) presented in [18,20] are not applicable to our case. We are therefore unable to compare our data with theory and we hope to return to this problem at another opportunity.

In conclusion of this section we note the peculiar change in the spectrum of lines ω_{30} and ω'_{30} ($\lambda = 4044/47$ Å) occurring at high laser and SRS powers (Fig. 4 a, b). There is a triplet structure at the edges of the line (along the slit height) while the center of the line has an essentially new form; it is difficult to provide a convincing interpretation of this fact.

4. CONCLUSION

The above interpretation of the observed effects does not profess to have a uniform degree of validity among its various aspects. A well established conclusion is that of the field origin of absorption line splitting at the $4S_{1/2} - 5P_{3/2,1/2}$ transition. Another basic conclusion concerning the significant role of four-photon scattering can be considered reliable only in relation to the broad "short-wave" line ω_{g5} . The role of four-photon processes in the remaining regions of the spectrum requires clarification in further experimental research.

Our results give rise to other more general conclusions. In the discussion of experimental data we repeatedly used concepts based on the perturbation theory that regards processes involving different numbers of photons as different or independent processes. One of the general conclusions of our work is that such a distinction becomes groundless when the emission intensity is high enough. Using the structure of the $\lambda = 4044$ Å absorption line as an example we see that one-, two-, and three-photon processes are "mixed up" in an intense resonance field. Under these conditions it is more appropriate to talk about a single process of violet absorption in which the line structure is interpreted as a result of field splitting of atomic levels. Such an approach is in full accord with the spirit of nonlinear spectroscopy [2] and we regard the obtained data as an experimental verification of one of its main theses.

APPENDIX

We consider the problem of a potassium atom interacting with electromagnetic plane waves of the following spectral composition: monochromatic wave Ω_R , G_R interacts with transition 1 - 2; waves Ω_2 , G_2 and Ω_3 , G_3 interact with transition 2 - 3; and quasi-monochromatic

fields $V_S(t)$, $V_{30}(t)$ interact with transition 0 - 1, 0 - 3. Fields Ω_R , G_R and Ω_j , G_j ($j = 2, 3$) correspond to laser and infrared fields, and $V_S(t)$ and $V_{30}(t)$ refer to the Stokes nitrobenzene SRS and violet emission. Equations for probability amplitudes a_l ($l = 0, 1, 2, 3$) are written as follows:

$$\begin{aligned} \dot{\hat{a}} &= i\hat{A}\hat{a} - i\hat{V}a_0, \quad \dot{a}_0 = -i\hat{V}^+\hat{a}, \\ \hat{a} &= \begin{pmatrix} a_1 \\ a_2 \\ a_3 \end{pmatrix}, \quad \hat{V} = \begin{pmatrix} V_S(t) \\ 0 \\ V_{30}(t) \end{pmatrix}, \end{aligned} \quad (\text{A.1})$$

$$\hat{A} = \begin{pmatrix} i\gamma_1 & G_R e^{i\Omega_R t} & 0 \\ G_R e^{-i\Omega_R t} & i\gamma_2 & G_2 e^{-\Omega_2 t} + G_3 e^{-i\Omega_2 t} \\ 0 & G_2 e^{i\Omega_2 t} + G_3 e^{i\Omega_2 t} & i\gamma_3 \end{pmatrix}.$$

Here γ_1 , γ_2 , γ_3 are the decay rates of levels 1, 2, 3. Substitution of variables

$$a_1 = e^{-i(\Omega_R - \Omega_2)t} b^1, \quad a_2 = e^{i\Omega_2 t} b_2, \quad a_3 = b_3 \quad (\text{A.2})$$

reduces (A.1) to

$$\begin{aligned} \dot{\hat{b}} &= i\hat{B}\hat{b} - i\hat{U}a_0, \quad a_0 = -i\hat{U}^+\hat{b}, \\ \hat{B} &= \begin{pmatrix} -\Omega_R + \Omega_3 + i\gamma_1 & G_R & 0 \\ G_R & \Omega_3 + i\gamma_2 & G_3 + G_2 e^{-i\Omega_2 t} \\ 0 & G_3 + G_2 e^{i\Omega_2 t} & i\gamma_3 \end{pmatrix}, \\ \hat{U} &= \begin{pmatrix} V_{30} e^{-i(\Omega_R - \Omega_2)t} \\ 0 \\ V_{20} \end{pmatrix}, \quad \Omega = \Omega_2 - \Omega_3 \end{aligned} \quad (\text{A.3})$$

Perturbation theory corresponds to a solution of system (A.3) by the method of successive approximations (for the initial condition $a_0(-\infty) = 1$), i.e., it assumes that all fields G and V_S , V_{30} are small. Under our experimental conditions this assumption is valid only in relation to V_S and V_{30} but not in relation to monochromatic fields G_R , G_2 , G_3 . Therefore only terms $i\hat{U}a_0$ and $i\hat{U}^+\hat{b}$ are considered in the following as small and are manipulated by the method of successive approximations.³⁾

Let $\hat{S}(t, t_0)$ be the fundamental matrix of the equation

$$\dot{\hat{S}} = i\hat{B}\hat{S}, \quad \hat{S}(t_0, t_0) = \hat{E}. \quad (\text{A.4})$$

Then with initial conditions $a_0(t_0) = 1$ we have

$$\hat{b} = -i \int_{t_0}^t \hat{S}(t, t') \hat{U}(t') dt' + \dots;$$

$$a_0 = 1 - \int_{t_0}^t \int_{t_0}^{t_1} \hat{U}^+(t_1) \hat{S}(t_1, t_2) \hat{U}(t_2) dt_1 dt_2 + \dots \quad (\text{A.5})$$

Matrix \hat{B} in (A.3) is periodic with period $2\pi/\Omega$. Therefore \hat{S} can be represented in the form [21]

$$\hat{S}(t, t_1) = \hat{\Phi}(t) \exp\{i\hat{\mu}(t - t_1)\} \hat{\Phi}^{-1}(t_1); \quad (\text{A.6})$$

$$\hat{\Phi}(t) = \sum_{-\infty}^{\infty} \hat{C}^{(m)} e^{-im\Omega t}, \quad \hat{\Phi}^{-1}(t) = \sum_{-\infty}^{\infty} \hat{D}^{(m)} e^{im\Omega t}, \quad (\text{A.7})$$

where $\hat{\mu}$ is a constant diagonal and $\hat{\Phi}(t)$ is a periodic function of the matrix. Using (A.5)–(A.7) we compute the spectral density of the work of field V_{30} . It turns out to be proportional to the expression

³⁾ Another model was used in [10]: nitrobenzene SRS is considered monochromatic and strong while the remaining fields are weak. The principal effect here, i.e., the splitting of the resonance level, is real if the SRS spectral width is smaller than the splitting. However the reverse relationship occurs in reality. Therefore the model adopted in [10] is inadequate and the conclusions of that work are invalid.

$$|V_{30}(\omega)|^2 \text{Re} \left\{ \sum_m \sum_{l=1}^3 \frac{C_{3l}^{(m)} D_{l3}^{(m)}}{\mu_l'' + i(\omega - \omega_{30} + \mu_l' + m\Omega)} \right\} \quad (\text{A.8})$$

According to (A.8) the atomic absorption spectrum is a set of equidistant triplets spaced $|\Omega| = |\Omega_2 - \Omega_3|$ apart. The characteristic roots μ_l , $l = 1, 2, 3$, determine the position of absorption maxima within each triplet. Standard methods can be used to compute μ_l to any desired accuracy. If we take G_{23} , $G_R \ll |\Omega|$, $\gamma_j \ll G$, and $|\Omega_3| \ll G_3$, relations that hold under conditions of our experiments, then

$$\mu_1 = -\Omega_R + \Omega_2 - \frac{G_R^2}{\Omega} + i\gamma_1, \quad (\text{A.9})$$

$$\mu_{2,3} = \frac{\Omega_3}{2} + \frac{G_R^2}{2\Omega} \pm G_3 + \frac{i}{2}(\gamma_2 + \gamma_3).$$

¹A. M. Bonch-Bruевич and V. A. Khodovoi, Usp. Fiz. Nauk 93, 71 (1967) [Sov. Phys.-Uspekhi 10, 637 (1968)].

²S. G. Rautian, Report to the All-Union Symposium on the Physics of Gas Lasers, Novosibirsk, 1969.

³S. Yatsiv, M. Rokni, and S. Barak, IEEE J. Quantum Electronics QE4, 900 (1968).

⁴S. Yatsiv, W. G. Wagner, G. S. Pinkus, and F. J. McClung, Phys. Rev. Lett. 15, 614 (1965).

⁵M. Rokni and S. Yatsiv, Phys. Lett. 24A, 277 (1967).

⁶P. P. Sorokin, N. S. Shiren, and J. K. Lankard, Appl. Phys. Lett. 10, 44 (1967).

⁷M. E. Movsesyan, N. N. Badalyan, and V. A. Iradyan, ZhETF Pis. Red. 6, 631 (1967) [JETP Lett. 6, 127 (1967)].

⁸M. Rokni and S. Yatsiv, IEEE J. Quantum Electronics QE3, 329 (1967).

⁹O. J. Lumpkin, P. P. Sorokin, and J. R. Lankard, Bull. Am. Phys. Soc. 12, 1054 (1967).

¹⁰O. J. Lumpkin, IEEE J. Quantum Electronics QE4, 226 (1968).

¹¹Yu. M. Kirin, D. P. Kovalev, S. G. Rautian, and R. I. Sokolovskii, ZhETF Pis. Red. 9, 7 (1969) [JETP Lett. 9, 3 (1969)].

¹²S. Yatsiv, M. Rokni, and S. Barak, Phys. Rev. Lett. 20, 1282 (1968).

¹³E. L. Lewis, M. M. Rebbeck, and J. M. Vaughan, Phys. Lett. 30A, 50 (1969).

¹⁴T. Jajima and K. Shimoda, Adv. Quant. Electr. Columbia Univ. Press, N. Y., London, 1961, p. 548.

¹⁵T. Ya. Popova, A. K. Popov, S. G. Rautian, and A. A. Feoktistov, Zh. Eksp. Teor. Fiz. 57, 444 (1969) [Sov. Phys.-JETP 30, 243 (1970)].

¹⁶J. D. Abella and H. Z. Cummins, J. Appl. Phys. 32, 1177 (1961).

¹⁷I. I. Sobel'man, Vvedenie v teoriyu atomnykh spektrov (Introduction to the Theory of Atomic Spectra), Fizmatgiz, 1963.

¹⁸D. N. Klyshko, Zh. Eksp. Teor. Fiz. 55, 1006 (1968) [Sov. Phys.-JETP 28, 522 (1969)].

¹⁹Yu. M. Kirin, S. G. Rautian, A. E. Semenov, and B. M. Chernobrod, ZhETF Pis. Red. 11, 340 (1970) [JETP Lett. 11, 226 (1970)].

²⁰B. Ya. Zel'dovich, Zh. Eksp. Teor. Fiz. 58, 1348 (1970) [Sov. Phys.-JETP 31, 723 (1970)].

²¹E. A. Coddington and N. Levinson, Theory of Ordinary Differential Equations, (Russ. Transl.), IIL, 1958.

Translated by S. Kassel